Available online at www.sciencedirect.com
SCIENCE DIRECT
Journal of Molecular Catalysis A: Chemical 251 (2006) 270–276
JOURNAL OF MOLECULAR CATALYSIS A: CHEMICAL
www.elsevier.com/locate/molcata

A functional phenoxazinone synthase model based on dioximatomanganese(II) Kinetics and mechanism of the catalytic oxidation of 2-aminophenols by dioxygen

Imola Cs. Szigyártó [a], Tatiana M. Simándi [a], László I. Simándi [a,*], László Korecz [b], Nóra Nagy [b]

[a] *Chemical Research Center, Institute of Surface Science and Catalysis, Hungarian Academy of Sciences, P.O. Box 17, H-1525 Budapest, Hungary*
[b] *Chemical Research Center, Institute of Structural Chemistry, Hungarian Academy of Sciences, P.O. Box 17, H-1525 Budapest, Hungary*

Available online 14 March 2006

Abstract

The dimeric dioximatomanganese(II) complex $[Mn_2(HL)_2](BPh_4)_2$ (**1**) (where H_2L is $[HON{=}C(CH_3)C(CH_3){=}NCH_2CH_2]_2NH$) dissociates to the monomer $[Mn(HL)]^+$ (**2**) upon dissolution in MeOH. Complex **2** is a functional phenoxazinone synthase model catalyzing the base-assisted oxidative dimerization of 2-aminophenol (H_3ap) to 2-amino-3*H*-phenoxazine-3-one (apx) by dioxygen under ambient conditions via an *o*-benzoquinone monoimine (bqmi) intermediate, which, however, cannot be directly detected due to its high reactivity. If H_3ap is replaced by 2-anilino-4,6-di-*tert*-butylphenol (**3**), a structural analog where the required positions are blocked, oxidation occurs without dimerization, affording the corresponding *N*-substituted *o*-quinone monoimine. Free radical intermediates were detected by ESR spectroscopy in both reactions. The kinetics of the catalytic oxidation of H_3ap was studied spectrophotometrically and the corresponding rate equation established. It is consistent with a mechanism involving the formation of a catalyst-H_2apO_2 ternary complex, which decomposes in the rate-determining step, generating a semiquinone monoimine undergoing noncatalytic oxidative dimerization to apx.
© 2006 Elsevier B.V. All rights reserved.

Keywords: 2-Aminophenol; 2-Anilino-4,6-di-*tert*-butylphenol; Phenoxazinone synthase; Semiquinone monoimine; ESR spectroscopy; Functional models

1. Introduction

The catalytic activation of dioxygen by transition metal complexes continues to attract interest [1] with special emphasis on modelling studies aimed at elucidation of oxidases, oxygenases, dehydrogenases and related metalloenzymes. Important substrate groups have been phenol and catechol derivatives, which provide valuable mechanistic information on processes in living organisms and are sometimes also of synthetic utility. Catechol dioxygenases are involved in the metabolism of aromatic compounds and low-molecular iron complexes are intensively studied as models of the enzyme active center [2–8]. In addition to dioxygenase activity, enzymes and models also exhibit catecholase activity, a feature of biological importance.

Related to catecholase activity is the ability of tyrosinase to promote the oxidation of 2-aminophenol derivatives to 2-amino-3*H*-phenoxazine-3-ones [9]. The enzyme phenoxazinone synthase is involved in the last stages of the biosynthesis of Actinomycin D [10,11] a naturally occurring antineoplastic agent, used clinically for the treatment of certain types of cancer [12]. According to Fig. 1, a 2-aminophenol derivative is catalytically converted to Actinomycin D in the presence of dioxygen and phenoxazinone synthase (also called *o*-aminophenol oxidase, EC 1.10.3.4), which is a type 2 copper-containing oxidase isolated from *Streptomyces* [13–16]. The mechanism of this six-electron oxidative coupling reaction has been studied using 2-aminophenol derivatives as substrates [14]. Nishinaga et al. [17] have studied the Co(salen) catalyzed oxidation of substituted H_3ap derivatives. Prati et al. investigated the copper-catalyzed oxidation of H_3ap to apx [18], and of the *m*- and *p*-isomers, which gave different products. Speier and coworkers reported the oxidation of H_3ap to 2-amino-3*H*-phenoxazine-3-one (apx) initiated by TEMPO [19,20] and recently studied the copper-catalyzed oxidative dimerization [21]. The electropolymerization of H_3ap yields insoluble films and some apx [22].

* Corresponding author. Tel.: +36 1 438 1126; fax: +36 1 438 1143.
E-mail address: simandi@chemres.hu (L.I. Simándi).

1381-1169/$ – see front matter © 2006 Elsevier B.V. All rights reserved.
doi:10.1016/j.molcata.2006.02.020

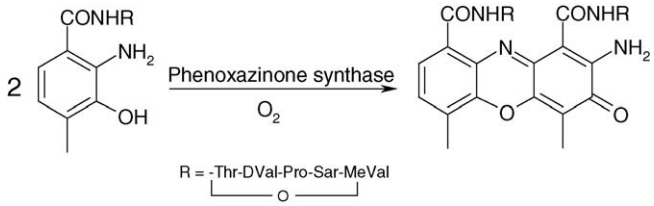

Fig. 1. Last stage of the biosynthesis of Actinomycin D.

The oxidation of *o*-substituted anilines by O_2 in the presence of cobalt salts [23] and of H_3ap catalyzed by a cobalt phthalocyanine derivative [24] have been reported.

We have previously investigated the catecholase [25,26] and phenoxazinone synthase [27,28] activity of cobaloxime(II). The structural analog ferroxime(II) also exhibits both catecholase [29,30] and phenoxazinone synthase [31] activity. Detailed mechanistic schemes based on kinetic and structural results and kinetic isotope effects have been reported [8,32]. A novel, catalytically active series of dioximatoiron(II) complexes has been structurally characterized by X-ray scattering in methanol solution [33].

According to our recent findings, the dioximatomanganese(II) dimer $[Mn_2(HL)_2](BPh_4)_2$ (**1**) {where H_2L is the quinquedentate dioxime ligand $HON{=}C(CH_3)C(CH_3){=}N{-}CH_2CH_2)_2NH$} acts as a catecholase mimic in methanol, converting 2,6-di-*tert*-butylcatechol to the corresponding *o*-quinone [34]. The catalytic activity is associated with the monomeric complex $[Mn(HL)]^+$ (**2**), which is formed instantaneously upon disolution of **1** in MeOH. We have now found that complex **1** is also a functional model for phenoxazinone synthase, converting 2-aminophenol (H_3ap) to 2-amino-3*H*-phenoxazine-3-one (apx). In the present paper kinetic studies on this functional model system are reported.

2. Experimental

2.1. Materials

$[Mn_2(HL)_2](BPh_4)_2$ was synthesized and characterized by the procedure developed by us [34]. 2-Aminophenol (Reanal, Hungary) was recrystallized from ^{i}PrOH (m.p. 177 °C). 2-Amino-3*H*-phenoxazin-3-one (m.p. 254–6 °C) as prepared by the cobaloxime(II) catalyzed oxidation of 2-aminophenol with O_2 [28]. 2-Anilino-4,6-di-*tert*-butylphenol was synthesized by a literature method [35].

2.2. Methods

The kinetic measurements were carried out by spectrophotometric monitoring of the increase in the concentration of the strongly absorbing 2-amino-3*H*-phenoxazin-3-one product ($\lambda = 432$ nm; $\varepsilon = 2.23 \times 10^4$ M^{-1} cm^{-1}).

In the kinetic experiments the oxidation was followed by recording the time evolution of UV–vis spectra on a Hewlett-Packard 8453 diode array spectrophotometer.

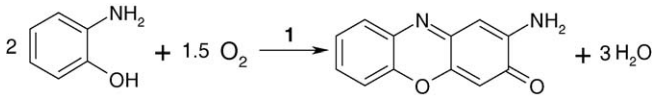

Fig. 2. Stoichiometric equation of the oxidation of H_3ap to apx in MeOH in the presence of complex **1**.

ESR spectra of reacting solutions were recorded on a Bruker ELEXYS E500 CW-EPR spectrometer, keeping the solution saturated with O_2 throughout the experiments. Spectra were accumulated over the initial 30 min of the reaction. Simulations of the spectra were carried out using the program developed by Rockenbauer and Korecz [36].

Electrospray ionization mass spectrometry (ESI-MS) was used to identify and monitor the species present in solution during the reaction [34].

3. Results and discussion

3.1. Catalytic oxidation of 2-aminophenol

The oxidation of H_3ap to 2-amino-3*H*-phenoxazin-3-one (apx) by O_2 in the presence of $[Mn_2(HL)_2](BPh_4)_2$ (**1**) (Fig. 2) takes place at room temperature in MeOH as solvent under air or and at 1 bar O_2.

The time evolution of the UV–vis spectra is shown in Fig. 3. The series of spectra reveal the oxidation of H_3ap to 2-aminophenoxazine-3-one (apx) as is shown by the increase of the 410–440 nm band characteristic of apx.

Special care was taken to determine the role of added triethylamine (TEA) and to establish catalysis by $[Mn(HL)]^+$, the monomeric complex formed upon dissolution of the dimer in MeOH. This was done as demonstrated by Fig. 4, which shows that oxidation of H_3ap takes place at a low rate when only TEA and the substrate are present (left section of smaller slope). Upon the addition of $[Mn(HL)]^+$ at the time indicated by an arrow, the

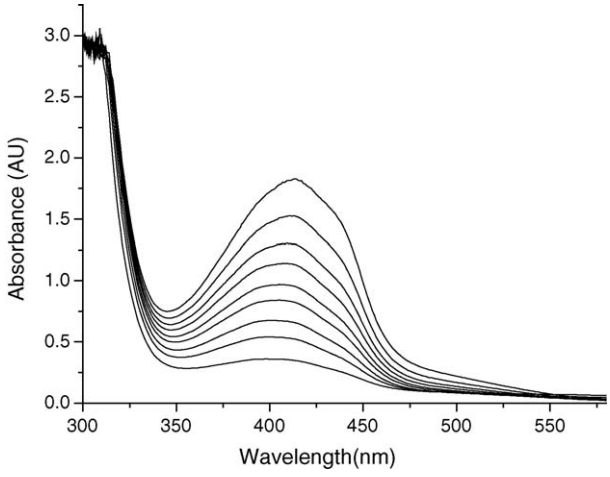

Fig. 3. Time evolution of the UV–vis spectra accompanying the oxidation of H_3ap to apx. $[1]_o = 2.6 \times 10^{-4}$ M; $[H_3ap]_o = 7.8 \times 10^{-3}$ M, $[TEA]_o = 3.9 \times 10^{-3}$ M; $T = 25$ °C, solvent MeOH. Wide band at 410–440 nm shows accumulation of apx. Spectra 1–5 (from bottom up) were taken at 60 s intervals, spectra 6–9 at 380, 470, 580 and 720 s, respectively.

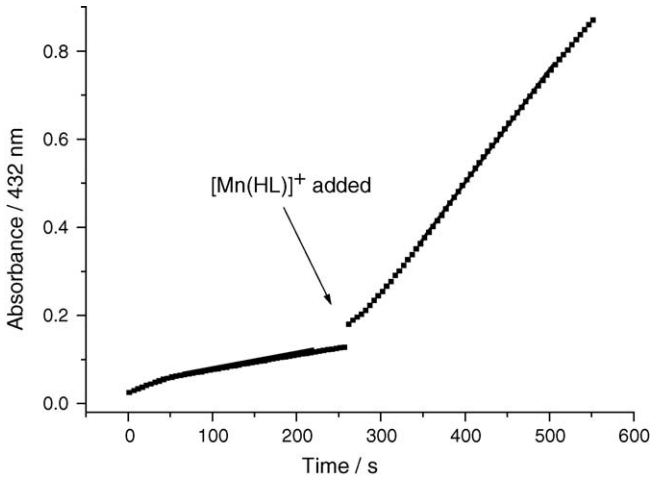

Fig. 4. Rate of the base-catalyzed oxidation (section 1) and its increase upon the addition of $[Mn(HL)]^+$ (section 2). Rate measured spectrophotometrically by monitoring the increase of absorbance at 432 nm (1 cm cell). Section 1: $[H_3ap]_o = 7.6 \times 10^{-3}$ M, $[TEA]_o = 3.8 \times 10^{-3}$ M; $T = 25\,^{\circ}C$; slope: 3.33×10^{-4} AU/s. Section 2: $[Mn]_o = 5.2 \times 10^{-4}$ M; slope: 2.56×10^{-3} AU/s.

rate significantly increases, demonstrating the catalytic effect of the complex. Thus oxidation of H_3ap takes place via parallel base-catalyzed and manganese-assisted routes.

3.2. ESR spectroscopy

The monitoring of the ESR spectra during the catalytic reaction provides information on the state of the catalyst complex in MeOH solution and on the reaction intermediates.

Upon dissolution of $[Mn_2(HL)_2](BPh_4)_2$ in methanol at 25 °C a characteristic six-line ESR signal immediately appears, indicating its dissociation to the monomeric $[Mn(HL)]^+$ complex (Fig. 5). Since the dimeric complex **1** was synthesized in, and crystallized from, MeOH by the addition of $NaBPh_4$ [34], followed by evaporation of the solvent, we conclude that in dilute

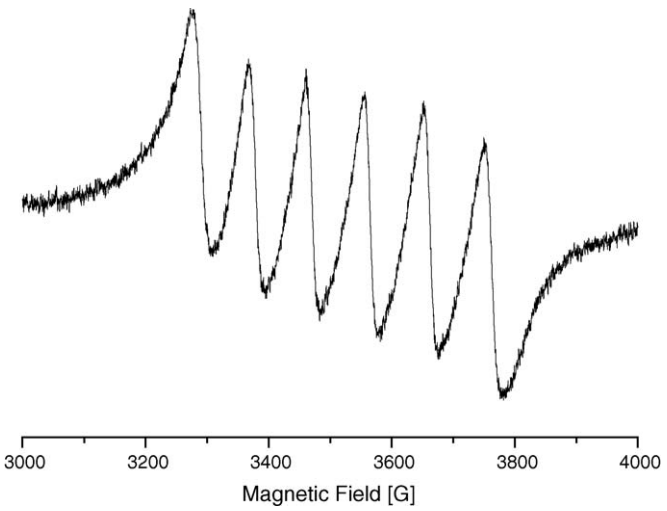

Fig. 5. Dissociation of the Mn^{II}/Mn^{II} dimer 1 into monomeric units 2: ESR spectrum of a 2.0×10^{-3} M solution of 1 in methanol immediately after dissolution at room temperature ($g = 2.007$, coupling constant = 96.4 G).

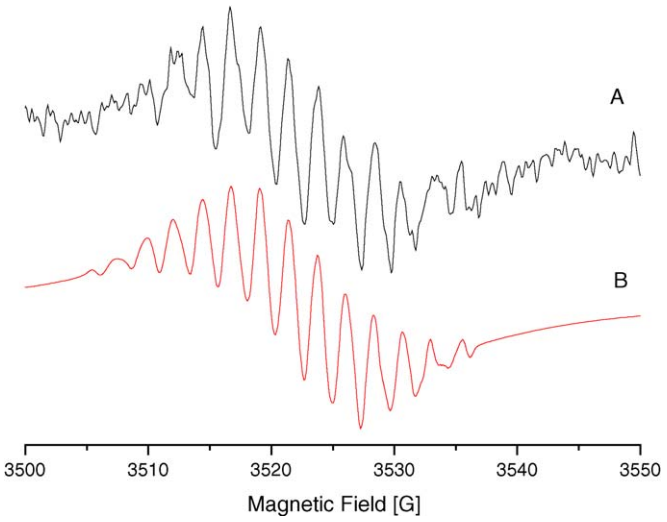

Fig. 6. ESR spectrum of a $Hapx^{\bullet}$ solution in which catalytic reaction (1) is taking place (A), and the simulated spectrum (B) using the parameters $g = 2.0049$, $1 \times a_N = 4.8$ G (2), $1 \times a_N = 4.5$ G (10), $a_{NH} = 2.8$ G, $a_{NH} = 2.7$ G, $a_H = 2.3$ G (4), $a_H = 2.1$ G, $a_H = 1.6$ G (1), solvent methanol, $T = 25\,^{\circ}C$, O_2 atmosphere. $[Mn]_o = 2.05 \times 10^{-3}$ M; $[H_3ap]_o = 3.00 \times 10^{-2}$ M; $[TEA] = 3.00 \times 10^{-2}$ M; solvent methanol, $T = 25\,^{\circ}C$. A: experimental spectrum; B: simulated spectrum.

solution **1** rapidly dissociates to the monomer, which remains stable for hours. A solution of **1** in acetonitrile exhibits a complex ESR spectrum, which is distinctly different from the spectrum in MeOH. After several hours a very weak six-line spectrum begins to appear superimposed on the background spectrum. Upon addition of MeOH to the acetonitrile solution the spectrum of the dimer is immediately replaced by the known six-line spectrum of the monomeric complex $[Mn(HL)]^+$.

The ESR spectrum of the catalytic solution in MeOH generating the apx product was monitored over the initial 30 min period of the reaction. Noise reduction by the accumulation of 200 successive spectra afforded a good quality spectrum of a free-radical intermediate (Fig. 6), superimposed on the much wider spectrum of the monomeric $[Mn(HL)]^+$. It corresponds to the free-radical intermediate $Hapx^{\bullet}$, as demonstrated by successful simulation using the software described in Ref. [36]. (For the formula of $Hapx^{\bullet}$, see the reaction mechanism.) The ESR spectrum of $Hapx^{\bullet}$ showed up immediately after the reactants were mixed and air was admitted (about 1 min). The initial poor resolution gradually improved as the number of accumulated spectra increased. The signal persisted for the period of observation at a steady state level, then a slow decrease of the signal intensity was observed.

The free radical $Hapx^{\bullet}$ is formed after the rate-determining step via a series of noncatalytic reactions shown in Fig. 7. The first of these steps is the conjugate addition of H_3ap to the catalytic oxidation product, bqmi, affording intermediate $C_{12}H_{12}N_2O_2$, which undergoes dehyrogenation followed by ring closure via intramolecular conjugate addition to yield $C_{12}H_{10}N_2O_2$. H-atom abstraction generates the free radical detected by ESR spectroscopy, $C_{12}H_9N_2O_2^{\bullet}$, and the transfer of another H-atom affords the product apx.

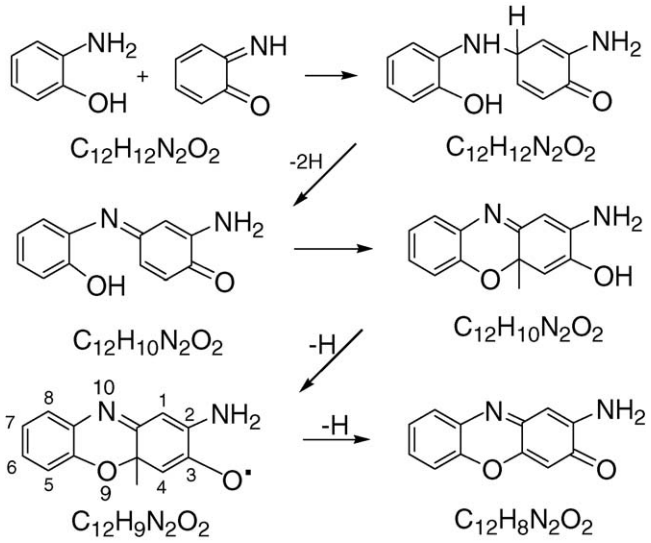

Fig. 7. Noncatalytic reactions leading to Hapx• and apx.

3.3. Kinetic measurements

The successive UV–vis spectra of the catalytic solutions in methanol were recorded in air atmosphere at 25 °C as a function of time. As the only product of H_3ap oxidation is apx, which is also the only absorbing species, the initial slopes of the absorbance versus time straight lines are readily converted to initial rates V_{in}. The initial rates of oxidation were determined as a function of the catalyst, substrate and triethylamine (TEA) concentration. The results are shown in Tables S1–S3 (see Supplementary information), where each value shown is the average of three individual runs reproducible to within ±3%. For brevity, the catalyst complex $[Mn(HL)]^+$ is denoted by Mn. At constant H_3ap concentration and O_2 pressure the initial rate was found to be proportional to the initial catalyst concentration denoted by $[Mn]_o$ (Fig. 8). When varying the initial concentration of H_3ap, a saturation type curve was observed (Fig. 9). A similar curve was obtained when varying the TEA concentration (Fig. 10).

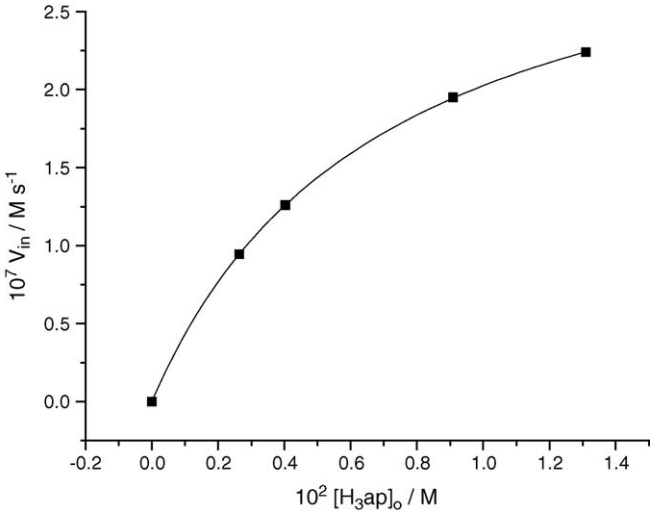

Fig. 9. Dependence of the initial rate on the substrate concentration. Conditions: $[Mn]_o = 2.65 \times 10^{-4}$ M, $[TEA] = 3.90 \times 10^{-3}$ M, $[O_2] = 2.20 \times 10^{-4}$ M, $T = 25\,^{\circ}C$, in air.

The kinetic pattern emerging from Figs. 8–10 is consistent with the reaction mechanism shown in (Eqs. (1)–(8)):

$$H_3ap + TEA \leftrightarrows H_2ap^- + HTEA^+ \qquad K_A/K_T \tag{1}$$

$$H_2ap^- + O_2 \leftrightarrows H_2apO_2^- \qquad K_B \tag{2}$$

$$H_2apO_2^- \rightarrow bqmi + HO_2^- \qquad RDS, k_B \tag{3}$$

$$[Mn_2(HL)_2]^{2+} + 2MeOH \rightarrow 2[(HL)Mn(MeOH)]^+ \qquad fast \tag{4}$$

$$[(HL)Mn^{II}(MeOH)]^+ + H_2apO_2^- \rightleftarrows \underset{(X)}{[(HL)Mn(H_2apO_2)]} + MeOH \qquad K_5 \tag{5}$$

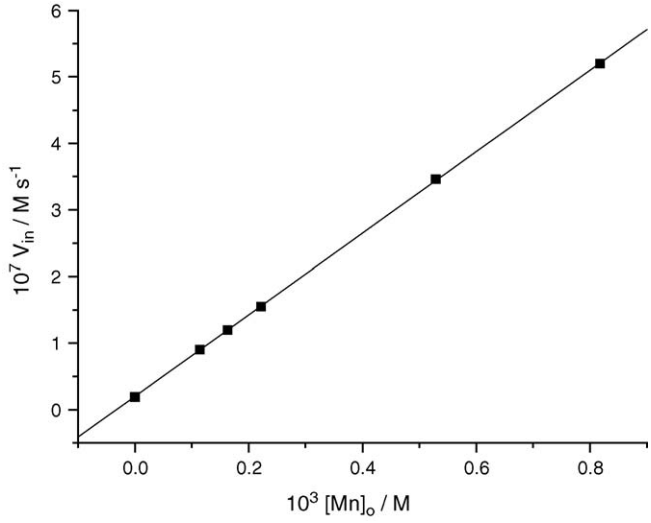

Fig. 8. Dependence of the rate of oxidation on the concentration of $[Mn(HL)]^+$. $[H_3ap]_o = 7.8 \times 10^{-3}$ M; $[TEA]_o = 3.9 \times 10^{-3}$ M, $[O_2] = 2.20 \times 10^{-4}$ M, $T = 25\,^{\circ}C$, in air.

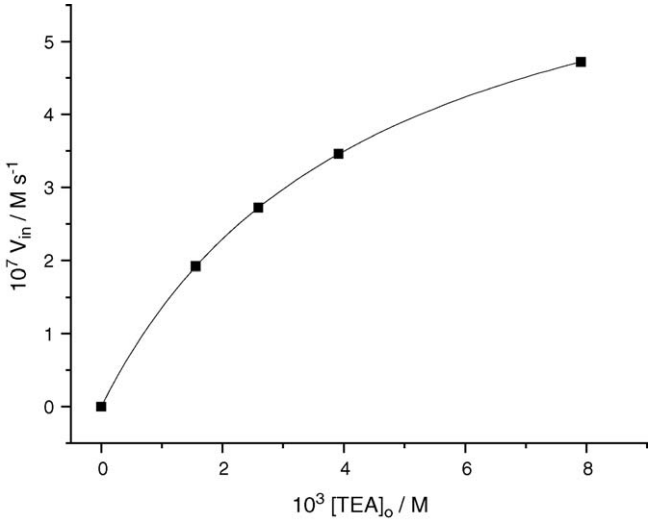

Fig. 10. Dependence of the initial rate on the TEA concentration. Conditions: $[Mn]_o = 5.32 \times 10^{-4}$ M, $[H_3ap] = 7.83 \times 10^{-3}$ M, $[O_2] = 2.20 \times 10^{-4}$ M, $T = 25\,^{\circ}C$, in air.

$$X \rightarrow [(HL)Mn^{II}(MeOH)]^{+} + bqmi + HO_2^{-} \qquad RDS, k_6 \tag{6}$$

$$2HO_2^{-} \rightarrow 2OH^{-} + O_2 \tag{7}$$

$$bqmi + H_3ap + O_2 \rightarrow apx + 2H_2O \qquad (fast\ step,\ cf.\ Fig.\ 7) \tag{8}$$

According to the proposed mechanism, the catalytic oxidation of H_3ap to bqmi takes place via two pathways, viz. (a) base-catalyzed oxidation involving steps (1)–(3), and (b) a combined base- and Mn-catalyzed route involving steps (1)–(3) followed by steps (4)–(6). Both pathways also involve reactions (7) and (8): repeated disproportionation (7) ensures that O_2 is reduced to water, whereas noncatalytic reactions (8) lead to the observed product apx. This mechanism is required by the fact that the base-catalyzed oxidation does occur in the absence of Mn catalyst, but no oxidation is observed if $[Mn_2(HL)_2]^{2+}$ is used without added base (see Fig. 4).

The base-catalyzed oxidation was run in the presence of TEA. It deprotonates H_3ap in equilibrium (1) to H_2ap^{-}, which binds O_2 in step (2) to yield a hydroperoxo species $H_2apO_2^{-}$ analogous to that generated in the base-catalyzed oxidation of catechol [3]. In the rate-determining step (3) $H_2apO_2^{-}$ generates benzoquinone monoimine (bqmi) and HO_2^{-}, which disproportionates to OH^{-} and O_2 in step (7).

The Mn-catalyzed path is due to the rapid solvolysis (4) of dimer **1** to produce the five-coordinate monomeric catalyst $[(HL)Mn^{II}(MeOH)]^{+}$, which binds $H_2apO_2^{-}$ in equilibrium (5) to generate intermediate X (see Fig. 11). The latter decomposes in rate-determining step (6), yielding bqmi and HO_2^{-}, as well as regenerating the starting $[(HL)Mn^{II}(MeOH)]^{+}$ catalyst.

The overall stoichiometry is achieved via repeated disproportionation of HO_2^{-} according to reaction (7).

After the rate-determining step, the bqmi produced reacts with O_2 in a series of steps, generating the free-radical intermediate Hapx$^{\bullet}$ detected by ESR spectroscopy (Fig. 6). The likely series of non-catalytic oxidation reactions leading to the apx product are shown in Fig. 7.

The kinetic equation consistent with the reaction mechanism (1)–(8) can be obtained by regarding step (4) as rapid and irreversible, in which all of the dimeric complex **1** dissociates to the monomer **2**. Steps (1), (2) and (5) behave as pre-equilibria and steps (3) and (6) are slow (rate-determining), whereas step (6) is fast. The initial rate of the combined base- and Mn-catalyzed paths (V_{in}) can be written as Eq. (9):

$$V_{in} = (k_B + k_6 K_5 [Mn]_o)\, K_B\, [H_2ap^{-}][O_2]_o \tag{9}$$

The mass balance and acid dissociation equilbria for H_3ap are given by Eqs. (10) and (11), whence expression (12) can be obtained for $[H_2ap^{-}]$:

$$[H_3ap]_o = [H_3ap] + [H_2ap^{-}] \tag{10}$$

$$K_{ap} = \frac{[H_3ap]}{[H_2ap^{-}][H^{+}]} \tag{11}$$

$$[H_2ap^{-}] = \frac{[H_3ap]_o}{(1 + K_{ap}[H^{+}])} \tag{12}$$

The effect of added TEA can be described in terms of equilibrium (1), mass balance (13) and protonation constant (14), yielding Eq. (15) for $[TEAH^{+}]$:

$$[TEA] = [TEA] + [TEAH^{+}] \tag{13}$$

$$K_T = \frac{[TEAH^{+}]}{[TEA][H^{+}]} \tag{14}$$

$$[TEAH^{+}] = \frac{[TEA]_o K_T [H^{+}]}{(1 + K_T[H^{+}])} \tag{15}$$

The proton concentration can be estimated by inserting Eqs. (12) and (15) into the charge balance Eq. (16), corresponding to equilibrium (1). The implicit expression (17) thus obtained can be rearranged to Eq. (18):

$$[TEAH^{+}] = [H_2ap^{-}] \tag{16}$$

$$\frac{[TEA]_o K_T [H^{+}]}{(1 + K_T[H^{+}])} = \frac{[H_3ap]_o}{(1 + K_{ap}[H^{+}])} \tag{17}$$

$$[H^{+}] = \frac{[H_3ap]_o}{K_T[TEA]_o} \frac{(1 + K_T[H^{+}])}{(1 + K_{ap}[H^{+}])} \tag{18}$$

Upon insertion of Eq. (18) into (12), we get Eq. (19), which can be simplified if we assume that $K_T\,[H^{+}] \ll 1$ and

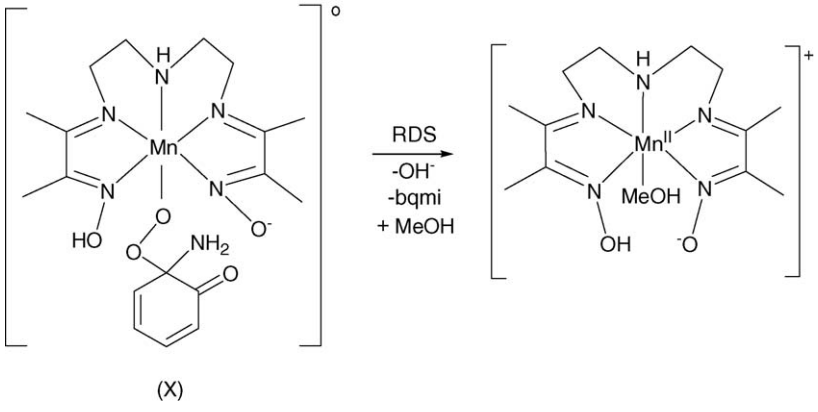

(X)

Fig. 11. Proposed structure and decomposition of the active intermediate X in the rate-determining step. X = $[(HL)Mn(H_2apO_2)]$.

$K_{ap}[H^+] \ll 1$:

$$[H_2ap^-] = \frac{[H_3ap]_o}{1 + (K_{ap}[H_3ap]_o)/(K_T[TEA]_o)\ ((1 + K_T[H^+]))/((1 + K_{ap}[H^+]))} \quad (19)$$

Insertion of the simplified expression for $[H_2ap^-]$ into Eq. (9) yields kinetic Eq. (20), which can be applied in the presence of TEA. The usual assumption for work with initial rates is accepted, i.e. the initial concentrations remain unchanged over the time-span of the measurements (subscript "o" refers to the initial value).

$$V_{in} = \frac{(k_B + k_6K_5[Mn]_o)K_B[O_2]_o[H_3ap]_o}{1 + (K_{ap}/K_T)[H_3ap]_o/[TEA]_o} \quad (20)$$

Non-linear least-squares fitting of expression (20) to the curves describing the dependence of V_{in} on the initial concentrations $[H_3ap]_o$ (Fig. 9) and $[TEA]_o$ (Fig. 10) affords the constants listed in Table 1. These constants can be used to calculate the slope of the V_{in} versus $[Mn]_o$ straight line and compare it with the experimental value.

The kinetic results are consistent with the reaction mechanism depicted by Eqs. (1)–(8).

3.4. Oxidation of 2-anilino-4,6-di-tert-butylphenol

Additional support for the proposed mechanism can be obtained from the oxidation of 2-anilino-4,6-di-*tert*-butylphenol (**3**) catalyzed by complex **2**. The monitoring of this reaction by ESR spectroscopy in MeOH has revealed H-atom abstraction to afford a relatively stable free radical intermediate (**4**) shown in Fig. 12. Under oxidative conditions **4** is further oxidized to the *N*-phenyl-4,6-di-*tert*-butyl-1,2-benzoquinone monoimine (**5**), rather than to apx, whose formation is prevented by the *N*-phenyl group. The ESR spectra of **4** can be readily generated in both MeOH and MeOD and are shown in Figs. 13 and 14, respectively, exhibiting the expected features due to D-substitution in MeOD.

On comparison of the ESR spectra in Figs. 13 and 14 it is apparent that in CH_3OD H–D substitution has taken place in both the OH and NH groups, as shown by the absence of $a_H = 3.98$ G. The two protons with coupling constants of 1.04 and 1.28 G are meta-protons in positions 3 and 5, respectively. The 18 protons with $a_H = 0.41$ and 1.37 G are due to the two di-*tert*-butyl groups in positions 4 and 6.

The ESR results confirm that the catalytic oxidation of H_3ap and **3** occur by similar mechanisms and the difference in products is consistent with the availability or blocking of sites required for dimerization.

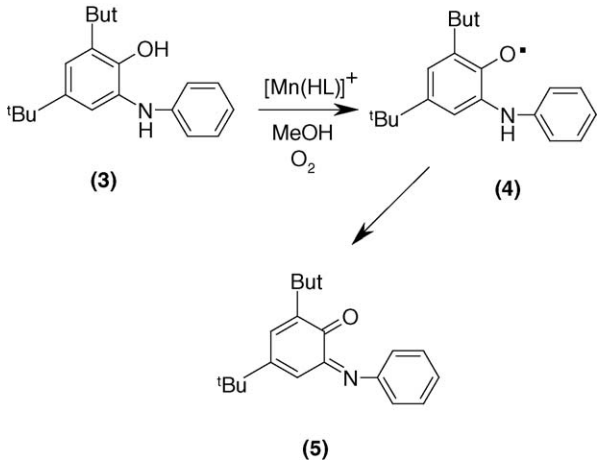

Fig. 12. Oxidation of the sterically hindered 2-anilino-4,6-di-*tert*-butylphenol (3) catalyzed by complex **2** in MeOH.

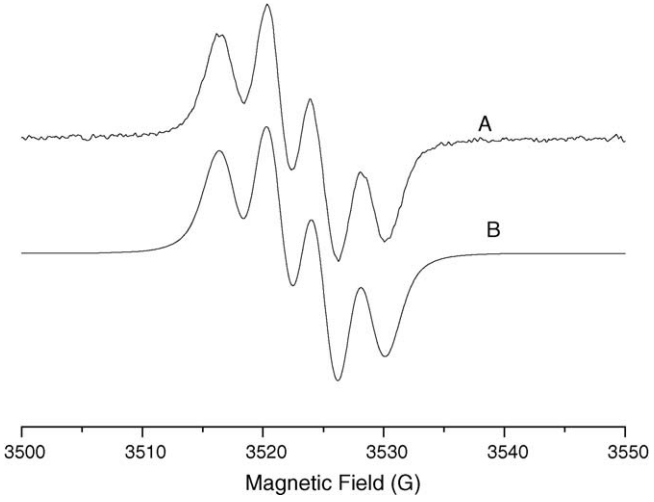

Fig. 13. ESR spectrum of the free-radical intermediate formed from 2-anilino-4,6-di-*tert*-butylphenol by H-atom abstraction (solvent MeOH). A: experimental spectrum; B: simulated spectrum with the parameters: $g = 2.0038$; $a_N = 3.51$ G; $a_H = 3.98$ G; $a_H = 1.04$ G (2H); $a_H = 0.41$ G (18H).

A series of Mn^{III} and Mn^{IV} complexes with coordinated free-radical ligand **4** and its ring-substituted derivatives have been synthesized and characterized by Wieghardt, Chaudhuri and coworkers [37,38]. These Mn^{IV} radical complexes catalyze the oxidation of 3,5-di-*tert*-butylcatechol with dioxygen.

Table 1
Rate and equilibrium constants determined from the fitting of Eq. (20) to the kinetic results

Source	K_{ap}/K_T	$k_6K_5K_B$ ($M^{-2}\ s^{-1}$)	k_B ($M^{-1}\ s^{-1}$)	Slope (s^{-1})
V_{in} vs. $[H_3ap]_o$ curve (Fig. 9)	0.55 ± 0.01	$(7.56 \pm 0.14) \times 10^2$	$(2.44 \pm 0.10) \times 10^{-2}$	n.a.
V_{in} vs. $[TEA]_o$ curve (Fig. 10)	0.56 ± 0.01			n.a.
V_{in} vs. $[Mn]_o$ line (Fig. 8) exp.	n.a.	n.a.	n.a.	$(6.13 \pm 0.12) \times 10^{-4}$
V_{in} vs. $[Mn]_o$ line (Fig. 8) calcd.	n.a.	n.a.	n.a.	$(6.11 \pm 0.12) \times 10^{-4}$

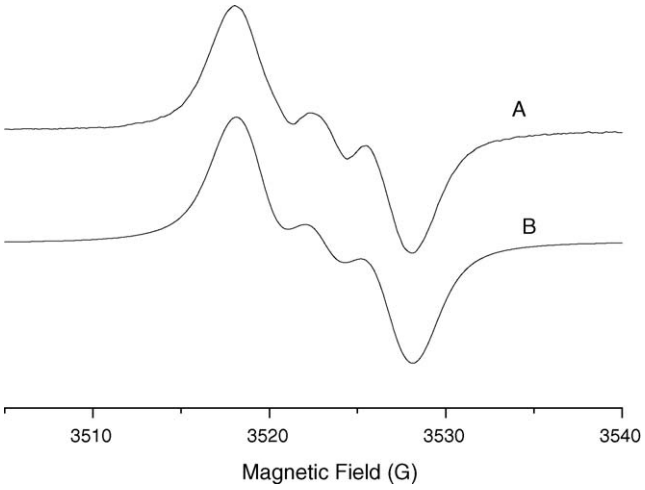

Fig. 14. ESR spectrum of the free-radical intermediate formed from 2-anilino-4,6-di-*tert*-butylphenol by D-atom abstraction (solvent MeOD). A: experimental spectrum; B: spectrum simulated with the parameters: $g = 2.0038$; $a_N = 3.43$ G; $a_H = 1.28$ G (2H); $a_H = 0.37$ G (18H).

4. Conclusion

In this work the dioximatomanganese(II) complex $[Mn(HL)]^+$ was demonstrated to act as a functional phenoxazinone synthase, which catalyzes the air oxidation of 2-aminophenol (H_3ap) in methanol to 2-amino-3*H*-phenoxazine-3-one (apx). Kinetic studies combined with ESR spectroscopy have shown that dioxygen activation and catalytic oxidation are restricted to the conversion of H_3ap to *o*-benzoquinone monoimine (bqmi), which occurs by a base-catalyzed and a manganese-assisted path. The active intermediate of the latter reaction is a complex consisting of the catalyst and the O_2 adduct of 2-aminophenolate(1−), decomposing to bqmi and the starting manganese(II) complex in the rate-determining step. From this point on, non-catalytic addition and oxidation steps take over. The last intermediate is a free radical directly oxidized to the apx product.

It is important that although triethylamine is needed for oxidation to occur, catalysis by $[Mn(HL)]^+$ is much faster than base-catalyzed oxidation alone. This is explained in terms of the proposed mechanism.

Work is in progress to further elucidate the scope and mechanisms of the catalytic activation of O_2 by manganese(II) complexes.

Acknowledgements

This work was supported by the Hungarian Science Fund (OTKA Grant T 034282) and by COST Chemistry Action D21 (Metalloenzymes and Chemical Biomimetics). We thank Prof. A. Rockenbauer for valuable discussions of the ESR results.

Appendix A. Supplementary data

Supplementary data associated with this article can be found, in the online version, at doi:10.1016/j.molcata.2006.02.020.

References

[1] J. Reedijk, E. Bouwman (Eds.), Bioinorganic Catalysis, 2nd ed., Marcel Dekker, New York, 1999.
[2] L.I. Simándi, Catalytic Activation of Dioxygen by Metal Complexes, Kluwer Academic Publishers, Dordrecht, Boston, London, 1992, p. 400.
[3] L.I. Simándi (Ed.), Advances in Catalytic Activation of Dioxygen by Metal Complexes, Kluwer Academic Publishers, Dordrecht, Boston, London, 2003, p. 336.
[4] T. Funabiki, in: L.I. Simándi (Ed.), Advances in Catalytic Activation of Dioxygen by Metal Complexes, Kluwer Academic Publishers, Dordrecht, Boston, London, 2003, pp. 158–226 (chapter 4).
[5] O. Gentschev, N. Moller, B. Krebs, Inorg. Chim. Acta 300 (2000) 442.
[6] M. Merkel, F.K. Muller, B. Krebs, Inorg. Chim. Acta 337 (2002) 308.
[7] L. Que Jr., Ref. [1], pp. 269–321.
[8] L.I. Simándi, T.M. Simándi, Z. May, G. Besenyei, Coord. Chem. Rev. 245 (2003) 87.
[9] O. Toussaint, K. Lerch, Biochemistry 26 (1987) 8567.
[10] U. Hollstein, Chem. Rev. 74 (1974) 625.
[11] E. Katz, H. Weissbach, J. Biol. Chem. 237 (1962) 882.
[12] E. Frei, Cancer Chemoter. Rep. 58 (1974) 49.
[13] C.E. Barry III, P.G. Nayar, T.B. Begley, J. Am. Chem. Soc. 110 (1988) 3333.
[14] C.E. Barry III, P.G. Nayar, T.B. Begley, Biochemistry 28 (1989) 6323.
[15] G.H. Jones, Antimicrob. Agents Chemother. 44 (2002) 1322.
[16] A.W. Smith, A. Camara-Artigas, C. Olea Jr., W.A. Francisco, J.P. Allen, Acta Cryst. D 60 (2004) 1453.
[17] K. Maruyama, T. Moriguchi, T. Mashino, A. Nishinaga, Chem. Lett. (1996) 819.
[18] L. Prati, M. Rossi, N. Ravasio, J. Mol. Catal. 79 (1992) 347.
[19] J. Kaizer, R. Csonka, G. Speier, J. Mol. Catal. A–Chem. 180 (2002) 91.
[20] J. Kaizer, R. Csonka, G. Speier, React. Kinet. Catal. Lett. 2 (2002) 367.
[21] T. Horváth, J. Kaizer, G. Speier, J. Mol. Catal. A–Chem. 215 (2004) 9.
[22] D. Goncalves, R.C. Faria, M. Yonashiro, L.O.S. Bulhoes, J. Electroanal. Chem. 487 (2000) 90.
[23] L.I. Simándi, S. Németh, N. Rumelis, J. Mol. Catal. 42 (1987) 357.
[24] Z. Szeverényi, E.R. Milaeva, L.I. Simándi, J. Mol. Catal. 67 (1991) 251.
[25] L.I. Simándi, T. Barna, Gy. Argay, T.L. Simándi, Inorg. Chem. 34 (1995) 6337.
[26] L.I. Simándi, T.L. Simándi, J. Chem. Soc. Dalton Trans. (1998) 3275.
[27] L.I. Simándi, T. Barna, L. Korecz, A. Rockenbauer, Tetrahedron Lett. 34 (1993) 717.
[28] L.I. Simándi, T. Barna, S. Németh, J. Chem. Soc. Dalton Trans. (1996) 473.
[29] T.L. Simándi, L.I. Simándi, J. Chem. Soc. Dalton Trans. (1999) 4529.
[30] L.I. Simándi, T.L. Simándi, J. Inorg. Biochem. 86 (2001) 432.
[31] T.M. Simándi, L.I. Simándi, M. Győr, A. Rockenbauer, Á Gömöry, Dalton Trans. (2004) 1056.
[32] T.M. Simándi, L.I. Simándi, Z. May, I.Cs. Szigyártó, Dalton Trans. (2005) 365.
[33] T. Megyes, Z. May, G. Schubert, T. Grósz, L.I. Simándi, T. Radnai, Inorg. Chim. Acta, in press.
[34] I.Cs. Szigyártó, L.I. Simándi, L. Párkányi, L. Korecz, G. Schlosser, Inorg. Chem., submitted for publication.
[35] P. Chaudhuri, C.N. Verani, E. Bill, E. Bothe, T. Weyhermüller, K. Wieghardt, J. Am. Chem. Soc. 123 (2001) 2213.
[36] A. Rockenbauer, L. Korecz, Appl. Magn. Reson. 10 (1996) 29.
[37] H. Chun, P. Chaudhuri, T. Weyhermüller, K. Wieghardt, Inorg. Chem. 41 (2002) 790.
[38] S. Mukherjee, T. Weyhermüller, E. Bothe, K. Wieghardt, P. Chaudhuri, Dalton Trans. (2004) 3842.